scientific data

Check for updates

OPEN

DATA DESCRIPTOR

Flexible joints for seismic-resilient design of masonry-infilled RC frames

Filip Manojlovski[1]✉, Enrico Tubaldi[2]✉, Vlatko Sheshov[1], Zoran Rakicevic[1], Aleksandra Bogdanovic[1], Julijana Bojadjieva[1], Antonio Shoklarovski[1], Angela Poposka[1], Dejan Ivanovski[1], Toni Kitanovski[1], Igor Markovski[1], Dejan Filipovski[1], Nikola Naumovski[1], Francesca Turchetti[2], Marko Marinković[3], Matija Bošković[3], Christoph Butenweg[4], Matija Gams[5], Nemanja Krtinić[5], Fabio Freddi[6], Ludovica Pieroni[6], Daniele Losanno[7], Fulvio Parisi[7], Prateek Dhir[8], Bartolomeo Pantó[8], Hamid Ahmadi[9], Jaymini Patel[9], Maximilian Schroeder[10], Udo Joachim Meyer[11], Britta Rosen[12] & Alessandro Lotti[13]

Masonry infills are among the most seismically vulnerable components in reinforced concrete frame structures. One promising mitigation strategy involves the use of rubber joints, which has shown potential in prior studies. However, further experimental and numerical investigations are needed to fully understand their effectiveness under realistic seismic conditions and to support evidence-based design. To address this, the EU-funded H2020 project FLExible JOInts for seismic-resilient design of masonry-infilled RC frames (FLEJOI) was conducted within the Engineering Research Infrastructures for European Synergies (ERIES) project. Two identical RC frame prototypes with brick infills and different rubber joint systems were constructed and tested at the Institute of Earthquake Engineering and Engineering Seismology – IZIIS in North Macedonia. The first system reduced panel stiffness and increased damping, while the second completely decoupled the infill from the frame. Both were subjected to extensive shaking table testing. This paper presents the resulting dataset, comprising detailed measurements from sensors monitoring the RC frames, infills, and joints – serving as a valuable benchmark for model validation and future research.

Background & Summary

Reinforced concrete (RC) buildings are among the most widespread building typologies worldwide. These structures typically incorporate masonry infill walls, which often represent their most vulnerable components. The failure of these walls can occur even during weak earthquakes, leading to significant direct losses (e.g., human casualties, repair costs) and indirect losses (e.g., downtime). The financial impact of infill damage can be substantial, with research indicating the cost of repairing damaged infills often surpasses that of structural components[1]. This highlights the significant need of modern societies for innovative technologies capable of improving the seismic performance and resilience of building structures while reducing the consequences of seismic events.

Significant research has been devoted in recent decades to developing technological solutions aimed at protecting infill walls from seismic damage due to in-plane loading, out-of-plane loading, or their interaction. Regarding the retrofitting of existing infill walls, a common approach is to enhance their resistance, employing a variety of solutions already available for masonry walls or developed specifically for this purpose (see e.g.[2–9]). For the design of new structures with infills, alternative techniques have been introduced, many of

[1]Institute of Earthquake Engineering and Engineering Seismology – IZIIS, Ss. Cyril and Methodius University in Skopje, Skopje, Republic of North Macedonia. [2]University of Strathclyde, Glasgow, United Kingdom. [3]University of Belgrade, Belgrade, Serbia. [4]RWTH Aachen University, Achen, Germany. [5]University of Ljubljana, Ljubljana, Slovenia. [6]University College London, London, United Kingdom. [7]University of Naples, Naples, Italy. [8]University of Durham, Durham, United Kingdom. [9]Tun Abdul Razak Research Centre - TARRC, Hertfort, United Kingdom. [10]Regupol, Bad Berleburg, Germany. [11]ZIEGEL German association of brick and tile industry, Herzogenrath, Germany. [12]SDA Engineering GmbH, Herzogenrath, Germany. [13]University of Trento, Trento, Italy. ✉e-mail: filipmanojlovski@iziis.ukim.edu.mk; enrico.tubaldi@strath.ac.uk

which were developed during the EU-funded project INSYSME[10]. These techniques aim to engineer infill walls with improved behaviour and reduced interaction with the building's structural components, compared to traditional infills. This objective can be achieved by increasing the flexibility of the infill panel and/or isolating it from the surrounding frame using flexible connections or sliding/frictional joints[11–21]. Among the various joint systems proposed, rubber joints have emerged as a particularly effective solution due to their adaptable stiffness and energy dissipation capacities, which can be tailored through the selection of appropriate materials and designs[11–17].

Previous experimental tests, carried out mainly within the INSYSME project[10], provided a proof of concept for the rubber joint technology. However, further experimental and numerical studies are required to validate the effectiveness of rubber joints under realistic seismic conditions and to advance knowledge on their design practices. To address this need, the H2020 EU-funded project "FLExible JOInts for seismic-resilient design of masonry-infilled RC frames (FLEJOI)" was conducted within the framework of Engineering Research Infrastructures for European Synergies (ERIES)[22]. The specific objective of the ERIES-FLEJOI project is to evaluate the effectiveness of two distinct flexible rubber joint systems designed to protect masonry infills and improve the seismic performance of RC buildings equipped with these systems. The first system investigated consists of compliant, soft, and highly dissipative horizontal joints developed by the Tun Abdul Razak Research Centre (TARRC) and placed within the infill panels, complemented by vertical rubber joints installed between the panel and frame columns[11–15]. The second system, known as INODIS, involves sliding/flexible joints placed at the interface between the infill panels and the frame[13,18–20]. The effectiveness of the two systems for infill wall protection was demonstrated through previous experimental tests under quasi-static conditions[12,23–25]. Thus, the primary goal of this study was to evaluate how the systems performed under dynamic loading imposed through a shaking table. It is noteworthy that shaking table tests have been performed before only on different infill wall protection systems, such as infill walls with sliding joints under out-of-plane loading[26,27], and on a RC frame prototype with internal infills and polyurethane joints[28].

Two identical infilled RC frames, each equipped with one of the two alternative rubber joint systems, were constructed at the Dynamic Testing Laboratory of the Institute of Earthquake Engineering and Engineering Seismology (IZIIS) in North Macedonia and subjected to a comprehensive series of shaking table tests. This article details the experimental campaign and provides extensive information on the properties of the tested prototypes, construction processes, instrumentation, testing procedures, and test data obtained from various sensors. The dataset presented herein serves as an essential resource for calibrating and validating numerical models, supporting further research on the seismic performance of RC frames incorporating masonry infills with rubber joints. Additionally, it enables direct comparison of two alternative infill design strategies and provides critical insights necessary for implementing sliding and decoupled infill strategies explicitly introduced in the second generation of Eurocodes, thus facilitating their practical application by engineering professionals.

Methods

Description of the tested prototypes. Figure 1 presents the two three-dimensional, single-storey, single-bay reinforced concrete (RC) frames with masonry infills and rubber joint systems, constructed and experimentally tested at the Institute of Earthquake Engineering and Engineering Seismology (IZIIS). These frames replicate the configuration developed within the INMASPOL Project, which investigated the performance of deformable polyurethane-based joints for the seismic protection of masonry infills[28]. Each frame measures 2.7×2.7 m in both orthogonal directions, with a total height of 3.3 m, and includes extended footing beams and a cantilevered top slab, as illustrated in Fig. 1. The structural system consists of four RC columns with square cross-sections ($200 \times 200\,mm^2$) and beams 200 mm in width, monolithically embedded within a 200 mm thick slab. The relatively small cross-sections of beams and columns were intentionally selected to reduce inertial loads transmitted to the shaking table in the infilled prototype. This limitation was necessary to prevent excessive base moments that could exceed the capacity of the shaking table under high-intensity seismic inputs.

Figure 2 illustrates the detailed geometry of the frame members along with the layout of the longitudinal and transverse reinforcement. The reinforcement detailing adheres to the capacity design principles prescribed in Eurocode 2 and Eurocode 8, ensuring appropriate ductility and strength hierarchy, following the design methodology reported by Rousakis[28].

The first configuration, denoted as Model 1 (Fig. 1a), incorporates a hybrid rubber joint system, consisting of (i) horizontal elastomeric joints dividing the infill panel into four subpanels (Type 1 T), and (ii) vertical rubber strips placed along the interface between the masonry infill and adjacent RC columns (Type 1E). This configuration represents a compliant and energy-dissipative system, specifically designed to increase the deformability of the infill and reduce the transmission of forces to the RC frame during seismic loading. The horizontal joints were manufactured by TARRC using a specially formulated high-damping rubber compound developed for the ERIES-FLEJOI project. Their main function is to accommodate the relative motion between the masonry subpanels and the main mode of deformation is shear. The vertical elastomeric strips were fabricated from recycled rubber and supplied by Isolgomma. Their function is to control the contact compressive stresses at the interface between the infill and the columns. As shown in Fig. 3, the horizontal joints were installed between two mortar layers and featured diagonal ribbing to enhance the mechanical bond with the mortar. The vertical joints were adhered to the column surface using silicone-based adhesive sealants. Figure 3a presents a construction detail showing the installation of these joints, while Fig. 3b displays the fully assembled Model 1. Notably, a traditional mortar interface – rather than a flexible joint – was used at the base and top slab connections to provide some restraint against out-of-plane displacements, in alignment with the system layout adopted in the INSYSME Project[10,12].

Model 2 (Fig. 1b) implements a fully decoupled joint system (Type 2), where flexible rubber interfaces are installed continuously along all four sides of the masonry panel. This configuration utilises a specialized rubber

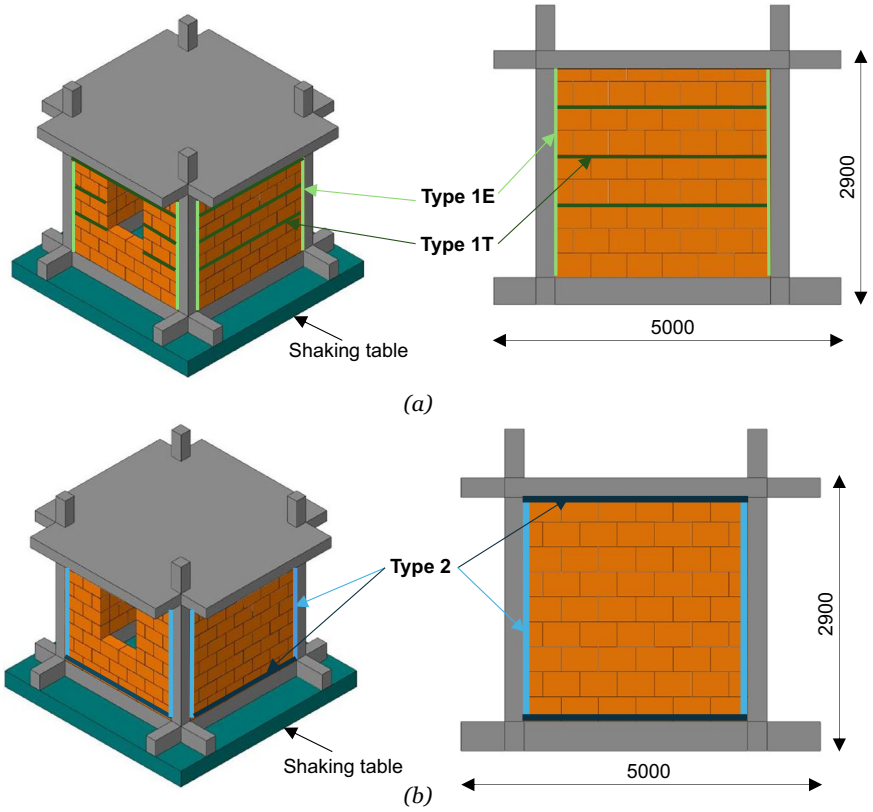

Fig. 1 (**a**) 3D view and geometric details with Type 1 joints. (**b**) 3D view and geometric details with Type 2 joints. (Dimensions are in mm).

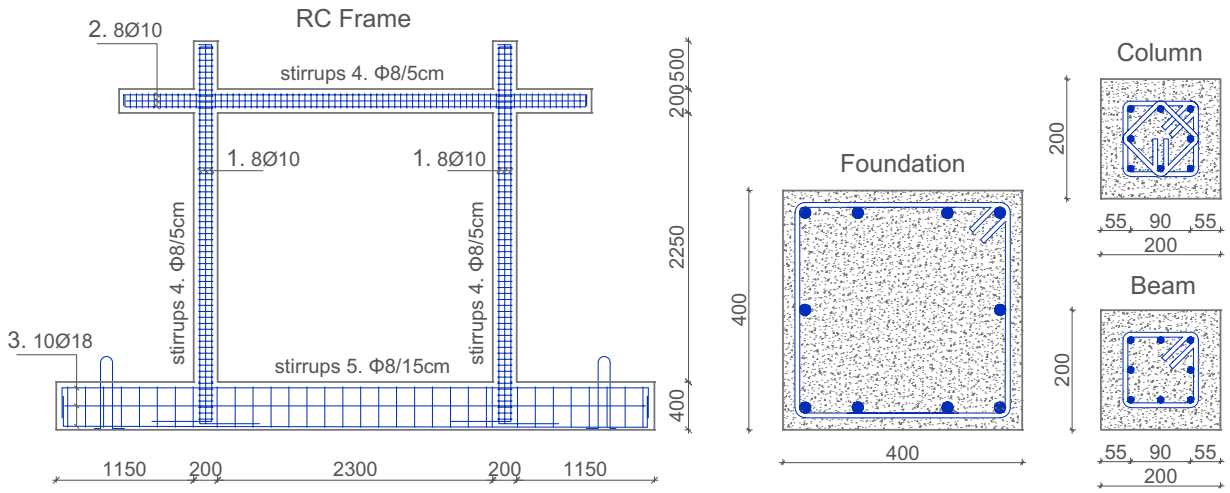

Fig. 2 Geometry and reinforcement details of tested RC frame. (Dimensions are in mm).

joint system developed by Marinković and Butenweg[16] and further improved by Milijaš *et al.*[24,25]. This rubber joint is now produced by Regupol and is commercially available. It is designed to achieve complete in-plane decoupling while maintaining adequate out-of-plane restraint. The rubber material used in the system exhibits low compressive and shear stiffness, allowing significant in-plane displacement capacity while effectively controlling out-of-plane movements. Figure 4 illustrates the assembly and construction process for Model 2. The out-of-plane restraint is achieved through a unique three-part joint layout: the outer rubber strips are bonded to the infill wall, while the central strip is adhered to the RC column, as shown in Fig. 5b. For the top and bottom connections to the RC slab and foundation beams, the joint is similarly subdivided into three layers – a middle elastomer layer and two outer rubber elements separated by a sliding plastic sheet, which allows in-plane displacement while maintaining structural separation (Fig. 5a). Figure 4a,b respectively illustrate the placement of

(a) (b)

Fig. 3 Model 1 rubber joints. (**a**) Type 1 rubber joints placement. (**b**) Completely built Model 1.

(a) (b)

Fig. 4 Model 2 rubber joints. (**a**) Type 2 rubber joints placement. (**b**) Completely built Model 2.

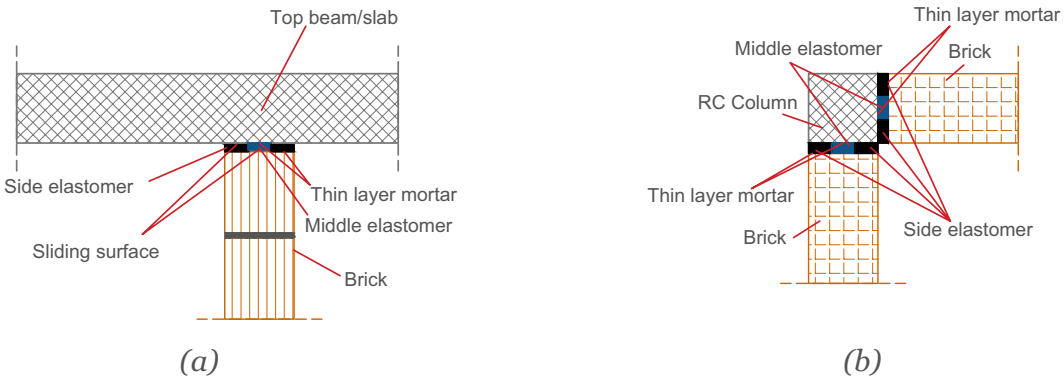

(a) (b)

Fig. 5 Type 2 joint system. (**a**) Wall to beam/foundation connection. (**b**) Wall to column connection.

the joint system and the completed Model 2 configuration. The conceptual aim of the Type 2 system is to render the infill panel a non-structural element in both design and behaviour, offering a robust, easily implemented, and installation-friendly solution for engineers. This system successfully eliminates infill-frame interaction by combining in-plane flexibility and out-of-plane anchorage, thereby protecting both the infill and the RC frame elements from damage during seismic events.

An additional mass composed of 18 steel ingots weighing 400 kg each (7200 kg total) was applied at the top of the slab of each model, resulting in an axial load ratio of the order of 3% in each column.

The masonry infill units used for both models were Porotherm 20 hollow clay bricks, produced by Wienerberger, with nominal dimensions of $375 \times 200 \times 238$ mm^3. These were assembled using horizontal mortar joints approximately 15 mm thick, while the vertical joints remained dry-stacked without mortar.

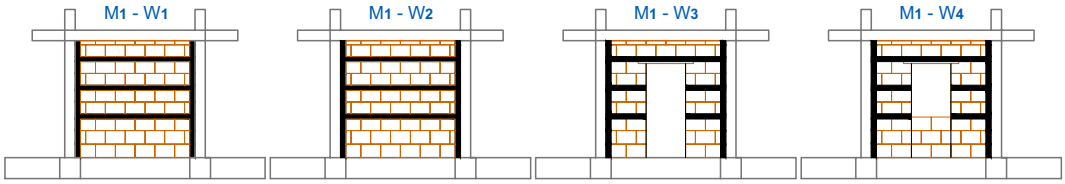

Fig. 6 Model 1. Infill walls and rubber joints placement.

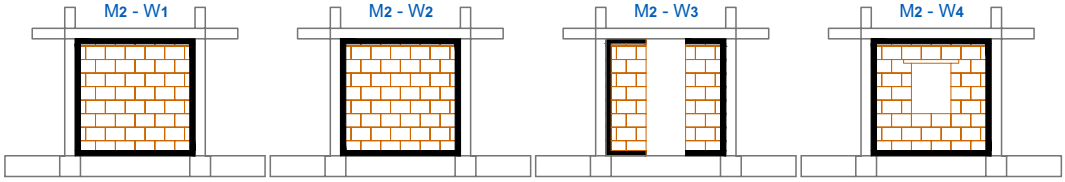

Fig. 7 Model 2. Infill walls and rubber joints placement. M = Model, W = Wall.

In terms of boundary configuration, both models included two fully infilled walls and two walls with window openings. The configuration of the infilled and open façades for Models 1 and 2 is depicted in Figs. 6, 7, respectively.

Experimental activities. The experimental campaign encompassed three main stages: (1) characterization tests of the constituent materials and joint components, (2) ambient vibration and impact hammer tests aimed at determining the dynamic properties of the structures, and (3) shaking table tests performed on both models to evaluate their dynamic behaviour and seismic response under specific earthquake time histories.

Materials characterisation tests. During the construction phase, material samples were collected for independent testing of mechanical properties. These tests aimed to quantify the strength of concrete, steel reinforcement, mortar, and masonry units used in both RC frames and infill systems.

Four concrete cubes, each measuring $150 \times 150 \times 150\,mm^3$, were cast during column construction and tested in compression according to the EN 12390-3 standard[29]. At 28 days, the recorded compressive strengths were 37.9 MPa, 37.7 MPa, 37.1 MPa, and 36.8 MPa, yielding an average value of 37.37 MPa.

Ten tensile specimens of 10 mm diameter longitudinal reinforcement bars were tested in accordance with EN ISO 15630-1[30]. The mean yield strength (f_y) was 578.3 MPa, while the mean ultimate tensile strength (f_u) was 667.3 MPa.

Two additional, non-standardized tests were performed to assess the compressive strength of the mortar and clay bricks used in the masonry infills. Due to the limited number of specimens, however, the results should be interpreted with caution as they lack statistical robustness.

For the mortar, three cube specimens ($150 \times 150 \times 150\,mm^3$) were prepared using the same ready-mix mortar applied during wall construction. These samples were tested in compression after 28 days of curing. The recorded compressive strengths were 20.2 MPa, 21.2 MPa, and 20.1 MPa, resulting in an average value of 20.5 MPa.

The compressive strength of the bricks was evaluated using two specimens, loaded along the direction of their internal ribs. A thin mortar layer was applied at the contact surfaces before loading. The measured ultimate compressive strengths were 5.81 MPa and 6.36 MPa, considerably lower than the nominal strength of 10 MPa indicated in the manufacturer's documentation. This discrepancy is attributed to the non-standard testing procedure and lack of conditioning of the brick specimens as required by standard protocols.

A comprehensive dataset of material properties, testing setups, and results is provided in the supplementary dataset files[31]. Among these files are also the results of the shear tests for characterising the high-damping rubber compound developed by TARRC for the horizontal joints in Type 1 system, of the compression tests on the Isolgomma's vertical joints. Regarding the rubber strips used in the Type 2 system, the results of their characterisation tests are provided in[16,25].

Operational modal analysis – ambient vibration tests. To investigate the dynamic characteristics of the models, including natural frequencies, damping ratios, and mode shapes, and monitor their evolution due to structural changes and damage, a series of ambient vibration and white noise excitation tests were carried out. The methodology is described in detail to allow reproducibility and facilitate interpretation of the recorded data.

Four distinct phases of dynamic testing were performed on both models. Phases 1 and 2 consisted of ambient vibration measurements taken during construction (bare frame) and immediately after infill installation (completed models). In Phase 3, the models were mounted on the shaking table, and random white noise excitations were applied. Phase 4 involved rotating the models 90° and repeating the measurements after the initial set of shaking table tests.

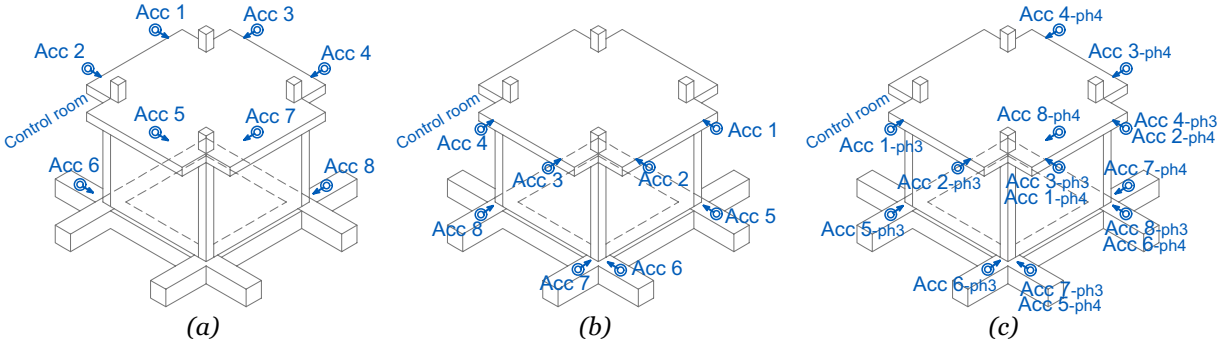

Fig. 8 Accelerometers for OMA. (**a**) Model 1 and Model 2, phase 1 – RC structure, phase 2 – with infills. (**b**) Model 1, phase 3 – placed on shaking table and phase 4 – rotated 90 degrees. (**c**) Model 2, phase 3 – placed on shaking table and phase 4 – rotated 90 degrees.

Throughout all testing phases, structural responses were recorded using accelerometers. The transducer layouts corresponding to each phase are illustrated in Fig. 8.

During ambient vibration tests, only the output response of the structure was recorded, enabling the application of output-only system identification techniques such as Operational Modal Analysis (OMA). The first OMA test was performed on the bare frames, while the second followed infill wall installation, enabling evaluation of the influence of masonry on global dynamic behaviour. Both tests preceded the shaking table campaign. It should be noted that boundary conditions can significantly affect modal parameter identification. For instance, the first model was temporarily supported on I-shaped timber beams (200 mm high, spaced 500–600 mm apart) with a 25 mm thick plywood cover, whereas the second model rested directly on ground-level wooden boards without intermediate beams.

For the random white noise tests, input excitation data from the shaking table were also recorded, allowing for both output-only (OMA) and input–output (Experimental Modal Analysis – EMA) processing. The excitation consisted of white Gaussian noise with a standard deviation of 0.01 g and constant power spectral density over the frequency range 1–45 Hz. These tests were conducted in both principal directions of the models (0° and 90°). The first, 0° test was executed prior to any seismic excitation. Subsequent tests were repeated after each major shaking table input, following the schedule outlined in Table 1. Tests in the 90° orientation were performed after completing all 0° direction experiments.

Shaking table and impact load tests. The shaking table testing campaign was conducted in two phases for each structural model. In Phase 1, the models were oriented such that the fully infilled walls were subjected to in-plane loading, aligned with the direction of seismic excitation, while the walls containing openings were exposed to out-of-plane loading, perpendicular to the excitation direction. In Phase 2, each model was carefully lifted, rotated by 90 degrees about its vertical axis, and repositioned on the shaking table. This resulted in the walls with openings being subjected to in-plane excitation, and the fully infilled walls to out-of-plane forces.

The testing program commenced with low-amplitude white noise excitations to evaluate the initial dynamic characteristics of the assembled system – serving as a complement to the results obtained from ambient vibration tests and operational modal analysis (OMA). Subsequently, ground motion records were imposed with increasing levels of intensity by scaling the input amplitude, simulating progressively stronger seismic demands.

For Model 1, three real earthquake records were used: Adana 1998 (Mw 6.3), Erzincan 1992 (Mw 6.6), and Umbria 2016 (Mw 6.2). These records were selected to reflect a range of frequency contents. For Model 2, the input set consisted of the Adana 1998 record and a synthetic accelerogram generated based on the Eurocode 8 elastic spectrum for Soil Type C. The inclusion of the synthetic record aimed to broaden the coverage of predominant frequencies and better represent design-level seismic actions.

In addition to the seismic simulations, impact hammer tests were performed before and after the shaking table tests to monitor changes in the dynamic characteristics of the infill walls, particularly in the out-of-plane direction. These tests employed Experimental Modal Analysis (EMA) techniques to quantify frequency shifts and stiffness degradation. For Model 1, the time interval between successive hammer impacts was maintained at 15 seconds, while for Model 2, the interval was extended to 30 seconds, optimizing signal capture and data clarity. The impact hammer strike locations are precisely indicated in Figs. 10, 19.

The full testing matrix – including all white noise tests, ground motion excitations, and hammer impacts – for Model 1 and Model 2 is summarized in Tables 1, 2, respectively. Each entry specifies the type of test conducted and includes additional notes and remarks relevant to each experimental run.

Instrumentation and transducers specifications. The dynamic tests were carried out using the shaking table facility at IZIIS, featuring a 5.0 m × 5.0 m platform with five degrees of freedom, actuated by two lateral and four vertical MTS hydraulic actuators. The system is controlled by an MTS Digital Controller 469D. The table has a maximum payload capacity of 40 tons and operates over a frequency range from 0.1 Hz to 50 Hz. In the horizontal direction, the platform allows displacements up to ± 125 mm and can reach accelerations of up to 3 g under zero payload conditions. In the vertical direction, the displacement capacity is ± 60 mm, with a maximum acceleration of 1.5 g, also under zero payload.

Test	Type of test	Description
	Model 1 – Phase 1	
1	*EMA – Hammer excitation*	Wall 1 – 42 points, at 30 s.
2	*EMA – Hammer excitation*	Wall 1 – 42 points, at 15 s.
3	*EMA – Hammer excitation*	Wall 3 – 47 points, at 30 s.
4	*EMA – Hammer excitation*	Wall 3 – 47 points, at 15 s.
5	*EMA – Hammer excitation*	Wall 2 – 8 points, at 30 s.
6	*EMA – Hammer excitation*	Wall 2 – 8 points, at 15 s.
7	EMA – ST random excitation	White noise 1 – 45 Hz, 0.01 g
8	**Seismic**	**Adana EQ. 10% [max 0.055 g]**
9	**Seismic**	**Erzincan EQ. 10% [max 0.065 g]**
10	**Seismic**	**Erzincan EQ. 20% [max 0.128 g]**
11	**Seismic**	**Adana EQ. 20% [max 0.123 g]**
12	**Seismic**	**Adana EQ. 50% [max 0.332 g]**
13	**Seismic**	**Erzincan EQ. 40% [max 0.268 g]**
14	EMA – ST random excitation	White noise 1 – 45 Hz, 0.01 g
15	*EMA – Hammer excitation*	Wall 1 – 42 points, at 15 s.
16	OMA – Rubber hammer excitation	Wall 1, random excitation
17	*EMA – Hammer excitation*	Wall 2 – 8 points, at 15 s.
18	**Seismic**	**Adana EQ. 100% [max 0.675 g]**
19	EMA – ST random excitation	White noise 1 – 45 Hz, 0.01 g
20	**Seismic**	**Umbria EQ. 100% [max 0.617 g]**
	Model 1 – Phase 2	
1	*EMA – Hammer excitation*	Wall 1 – 42 points, at 30 s.
2	*EMA – Hammer excitation*	Wall 2 – 8 points, at 30 s.
3	*EMA – Hammer excitation*	Wall 3 – 47 points, at 30 s.
4	EMA – ST random excitation	White noise 1 – 45 Hz, 0.01 g
5	**Seismic**	**Adana EQ. 10% [max 0.062 g]**
6	**Seismic**	**Erzincan EQ. 10% [max 0.065 g]**
7	**Seismic**	**Erzincan EQ. 20% [max 0.128 g]**
8	**Seismic**	**Adana EQ. 20% [max 0.132 g]**
9	**Seismic**	**Adana EQ. 50% [max 0.314 g]**
10	**Seismic**	**Erzincan EQ. 40% [max 0.267 g]**
11	EMA – ST random excitation	White noise 1 – 45 Hz, 0.01 g
12	*EMA – Hammer excitation*	Wall 1 – 42 points, at 30 s.
13	*EMA – Hammer excitation*	Wall 2 – 8 points, at 30 s.
14	*EMA – Hammer excitation*	Wall 3 – 47 points, at 30 s.
15	**Seismic**	**Adana EQ. 100% [max 0.728 g]**
16	EMA – ST random excitation	White noise 1 – 45 Hz, 0.01 g
17	**Seismic**	**Umbria EQ. 80% [max 0.51 g]**
18	EMA – ST random excitation	White noise 1 – 45 Hz, 0.01 g
19	*EMA – Hammer excitation*	Wall 1 – 42 points, at 30 s.
20	*EMA – Hammer excitation*	Wall 2 – 8 points, at 30 s.
21	*EMA – Hammer excitation*	Wall 3 – 47 points, at 30 s.

Table 1. List of performed tests – Model 1.

For the modal impact tests, a PCB Piezotronics modal hammer (Model 086D20) with a grey super soft tip (Model 084B60) was employed. This hammer features a measurement range of ±22,240 N peak and a resonant frequency of at least 12 kHz, enabling accurate dynamic excitation of the structural models.

The instrumentation installed on the models included various sensor types to capture different structural response parameters. Acceleration was measured using PCB Piezotronics accelerometers (Model 333B, variants 30–50) and Kistler accelerometers (Model 8712A5M1), all in range from 5 g to 50 g. Only the ambient vibrations measurements required for operational modal analysis were measured by 0.5 g range accelerometers PCB ICP 393B12. Displacements were measured using linear potentiometers (LP) from Micro-Epsilon (Model WDS-500-P60-SR-U) and linear variable differential transformers (LVDTs) from MacroSensors (Model DC750). Strain measurements were obtained using KYOWA strain gauges (Model KFGS-5-120-C1-11) with a gauge length of 5 mm.

The exact locations of all sensors are illustrated in Figs. 12–14 for Model 1 – Phase 1; Figs. 15–17 for Model 1 – Phase 2; Figs. 21–23 for Model 2 – Phase 1; and Figs. 24–26 for Model 2 – Phase 2. For the impact hammer

Test	Type of test	Description
	Model 2 – Phase 1	
1	*EMA – Hammer exc.*	Wall 1 – 8 points, at 30 s.
2	*EMA – Hammer exc.*	Wall 2 – 42 points, at 30 s.
3	*EMA – Hammer exc.*	Wall 3 – 44 points, at 30 s.
4	EMA – ST random exc.	White noise 1 – 45 Hz, 0.01 g
5	**Seismic**	**Adana EQ. 10% [max 0.065 g]**
6	EMA – ST random exc.	White noise 1 – 45 Hz, 0.01 g
7	**Seismic**	**Adana EQ. 20% [max 0.122 g]**
8	EMA – ST random exc.	White noise 1 – 45 Hz, 0.01 g
9	**Seismic**	**Generated EQ. 30% [max 0.181 g]**
10	EMA – ST random exc.	White noise 1 – 45 Hz, 0.01 g
11	**Seismic**	**Generated EQ. 60% [max 0.322 g]**
12	EMA – ST random exc.	White noise 1 – 45 Hz, 0.01 g
13	*EMA – Hammer exc.*	Wall 1 – 8 points, at 30 s.
14	*EMA – Hammer exc.*	Wall 2 – 42 points, at 30 s.
15	*EMA – Hammer exc.*	Wall 3 – 44 points, at 30 s.
	Model 2 – Phase 2	
1	EMA – ST random exc.	White noise 1 – 45 Hz, 0.01 g
2	**Seismic**	**Adana EQ. 10% [max 0.06 g]**
3	EMA – ST random exc.	White noise 1 – 45 Hz, 0.01 g
4	**Seismic**	**Adana EQ. 30% [max 0.17 g]**
5	EMA – ST random exc.	White noise 1 – 45 Hz, 0.01 g
6	**Seismic**	**Adana EQ. 40% [max 0.25 g]**
7	EMA – ST random exc.	White noise 1 – 45 Hz, 0.01 g
8	**Seismic**	**Adana EQ. 50% [max 0.3 g]**
9	EMA – ST random exc.	White noise 1 – 45 Hz, 0.01 g
10	*EMA – Hammer exc.*	Wall 1 – 8 points, at 30 s.
11	*EMA – Hammer exc.*	Wall 2 – 42 points, at 30 s.
12	*EMA – Hammer exc.*	Wall 3 – 44 points, at 30 s.

Table 2. List of performed tests – Model 2.

tests the accelerometer setup is shown on Fig. 11 for Model 1 and Fig. 20 for Model 2. Further technical details, sensor locations, and naming conventions are included in the accompanying dataset[31].

The data acquisition system used during shaking table tests was based on a National Instruments PXI-1006 chassis, outfitted with nine NI PXI-4472 dynamic signal acquisition modules. This system enabled real-time acquisition of acceleration, displacement, and force signals from the installed sensors, as well as reference and feedback signals for acceleration and displacement from the MTS control system. The PXI system supported high-resolution, synchronized multi-channel data acquisition at a sampling rate of 1000 samples per second, ensuring reliable and accurate representation of the structural response.

For strain gauge acquisition, a modular NI cDAQ-9188 chassis was employed, fitted with eight NI 9237 bridge input modules. These modules provide integrated excitation and signal conditioning and are optimized for high-speed and high-accuracy strain measurement, essential for capturing the material behaviour under dynamic loading.

Both PXI and cDAQ systems were synchronized using a shared trigger signal sourced from the shaking table controller, guaranteeing accurate time alignment across all sensor channels.

Additionally, ambient vibration data used for Operational Modal Analysis (OMA) were collected using a dedicated NI cDAQ-9178 system equipped with four NI 9234 dynamic signal acquisition cards. These cards are tailored for vibration and acoustic measurements and were operated at a higher sampling rate of 2000 Hz to capture low-amplitude dynamic responses effectively.

The entire acquisition setup was designed for flexible deployment across multiple testing phases and ensured consistent, high-fidelity data acquisition across all sensor types.

A commercial Digital Image Correlation (DIC) system – Zeiss Aramis Adjustable 24 M[32] was also used to monitor displacement and strain fields on one side of each model – the side subjected to in-plane loading. The system employed two 24 MP resolution cameras to capture full-field 3D displacement data. The cameras were positioned 2804 mm from the specimen surface, spaced 1210 mm apart, and oriented with an inter-camera angle of 17.5°. Image acquisition was performed at full resolution with a frame rate ranging between 70 and 100 Hz, depending on the duration of each test. Post-processing was completed using proprietary software – Zeiss Inspect Correlate 2023[33] provided by the DIC system manufacturer. For Model 1, DIC data were acquired for selected earthquake records (tests 12 and 20), while for Model 2, the DIC system was employed during all shaking table runs.

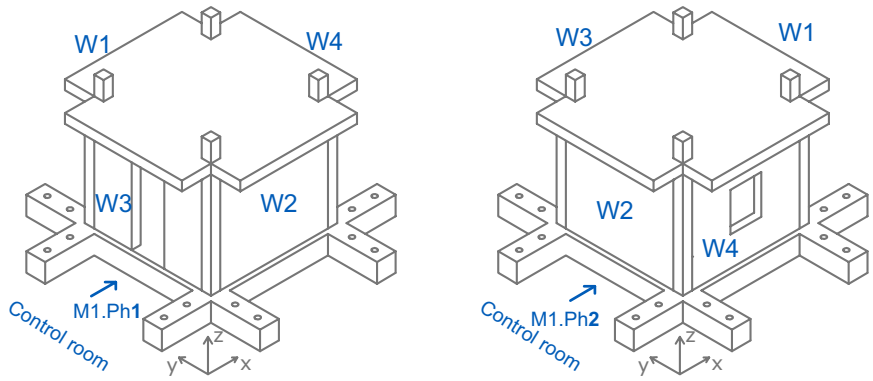

Fig. 9 Model 1. Direction of excitation of both phases and wall nomenclature. Model 1 - Impact hammer tests.

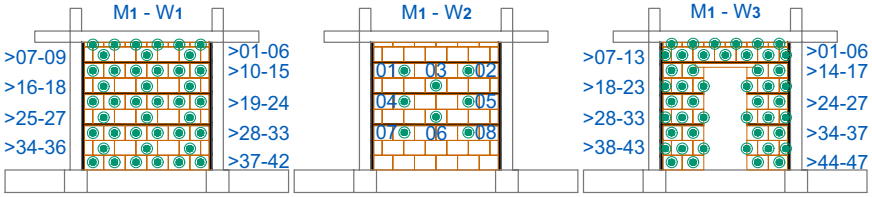

Fig. 10 Model 1. Impact hammer tests hitting points (inside).

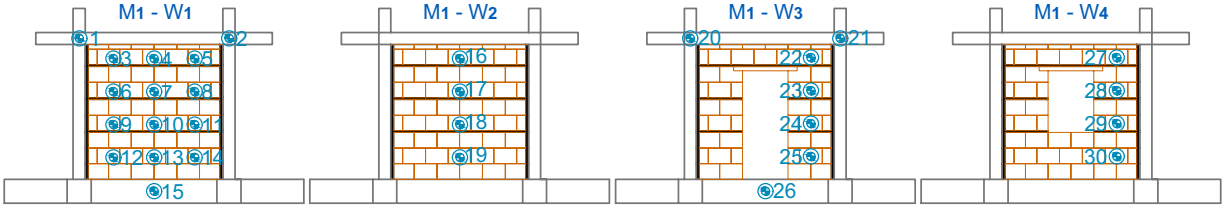

Fig. 11 Model 1. Instrumentation setup – Impact hammer tests. Positions of accelerometers (ACC). Model 1 – Shaking table tests – *Phase 1*.

Model 1 testing phases and instrumentation setup. The excitation directions for both testing phases, along with the wall nomenclature for Model 1, are illustrated in Fig. 9.

Model 2 testing phases and instrumentation setup. The excitation directions for both testing phases, along with the wall nomenclature for Model 2, are illustrated in Fig. 18.

Data Records

The dataset is available at the public repository Zenodo[31]. This repository was established in accordance with the ERIES Transnational Access Agreement, which mandates that the complete dataset generated during the experimental campaign be made publicly accessible to other users.

The project dataset is organized into five main folders. The project dataset is organized into five main folders. The first folder, titled "Drawings and Construction Phase Photos," contains detailed photographs documenting the construction process of both RC frame models, including all stages of reinforcement placement, masonry infill installation, and final assembly. It also holds the original vector structural drawings from the models.

The second folder, "Material Characterisation Tests," is divided into six subfolders, each corresponding to a specific material tested during the campaign: bricks, concrete for columns, mortar, reinforcement, and rubber joints, with an additional summary table compiling key mechanical properties. All data files are clearly labelled, allowing intuitive access to the desired information.

The third folder, "Shaking Table Testing," includes all seismic test data obtained from the shaking table and impact hammer experiments. It is structured into four subfolders: Model 1, Model 1 Rotated, Model 2, and Model 2 Rotated. Each subfolder contains test recordings in TDMS format[34,35], photo and video documentation of the setup, and clearly labelled strain gauge data files. A separate section provides tabulated information on the instrumentation layout and sensor positions used throughout the testing.

Fig. 12 Model 1. Instrumentation setup – Phase 1 – photos.

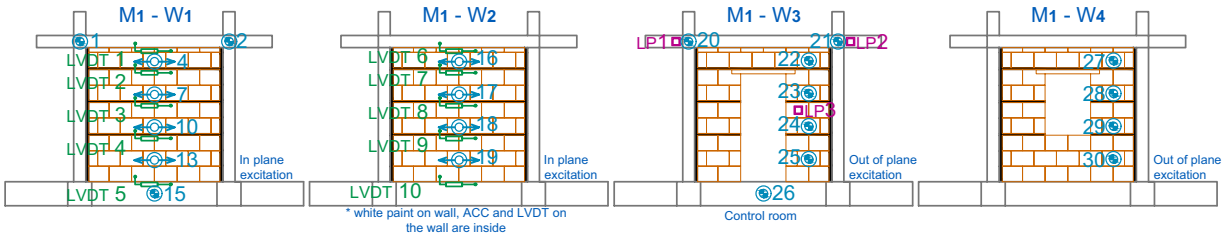

Fig. 13 Model 1. Instrumentation setup – Phase 1. Positions of accelerometers (ACC), linear potentiometers (LP) and linear variable differential transformers (LVDT).

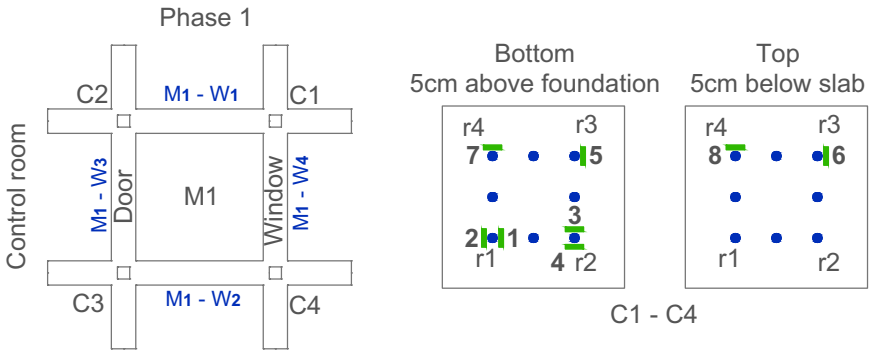

Fig. 14 Model 1. Instrumentation setup, Strain Gauges – Phase 1. *Model 1 – Shaking table tests (rotated model 90 degrees) – Phase 2.*

The fourth folder, "Shaking Table – DIC Data," contains displacement data from Digital Image Correlation (DIC) measurements. It is divided by model and direction of testing: Model 1 Direction 1, Model 2 Direction 1, and Model 2 Direction 2. Each subfolder includes figures showing the tracked points and figures showing the .csv[36] files listing the displacement values recorded during specific seismic input tests, named accordingly.

Fig. 15 Model 1. Instrumentation setup – Phase 2 – photos.

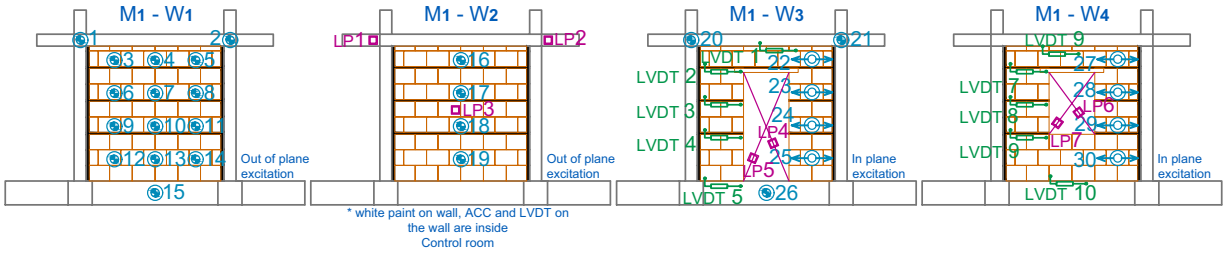

Fig. 16 Model 1. Instrumentation setup – Phase 2. Positions of accelerometers (ACC), linear potentiometers (LP), and linear variable differential transformers (LVDT).

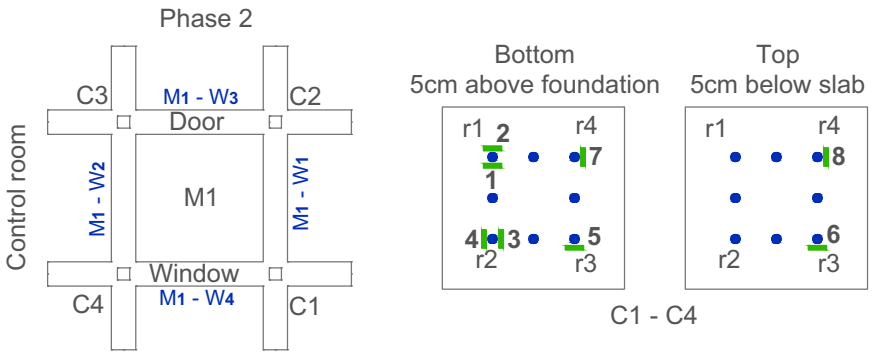

Fig. 17 Model 1. Instrumentation setup, Strain Gauges – Phase 2.

The fifth folder, "Dynamic Characteristics – Ambient Vibrations," includes photos from Operational Modal Analysis (OMA) conducted on bare and infilled frames in various configurations, along with corresponding measurement data stored in TDMS format[34,35]. The subfolders are organized to reflect the different test setups, including both initial and rotated model positions.

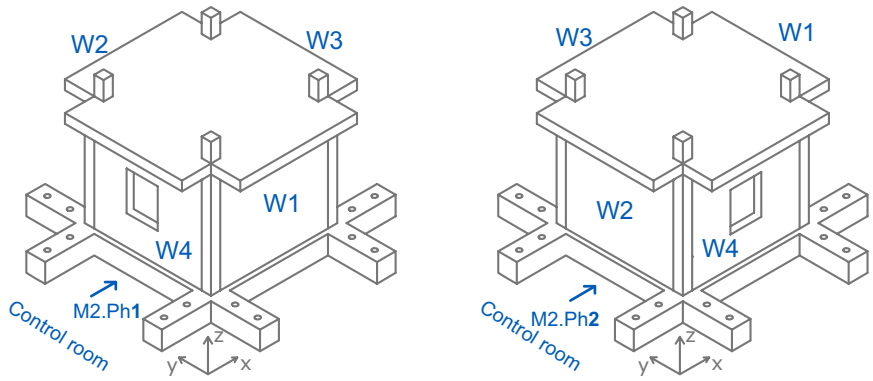

Fig. 18 Model 2. Direction of excitation of both phases and wall nomenclature. Model 2 - Impact hammer tests.

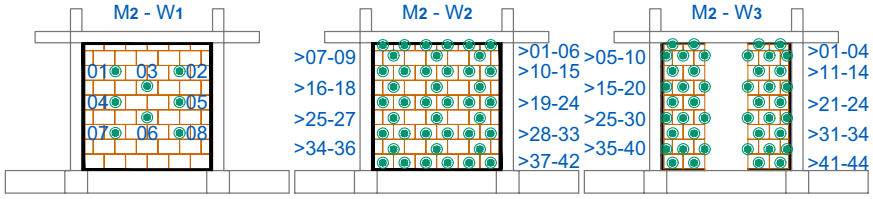

Fig. 19 Model 2. Impact hammer tests hitting points (inside).

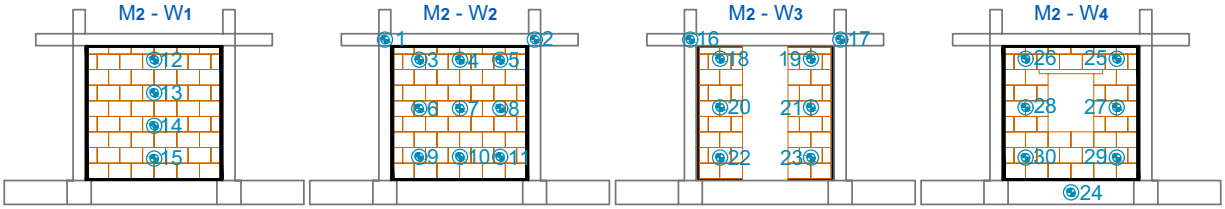

Fig. 20 Model 2. Instrumentation setup – Impact hammer tests. Positions of accelerometers (ACC). Model 2 – Shaking table tests – *Phase 1*.

All records from the shaking table and impact hammer tests were acquired using a synchronized data acquisition system operating at a sampling rate of 1000 samples per second whereas for the ambient vibration measurements, a higher sampling rate of 2000 samples per second was used. With the exception of accelerometer signals from the seismic tests and experimental modal analysis (EMA) using white noise, all transducer data are provided as raw TDMS files. The accelerometer data from seismic and EMA tests were post-processed using a bandpass filter in the frequency range of 0.5 to 35 Hz to reduce noise and enhance signal clarity.

Technical Validation

All transducers – including accelerometers, linear variable differential transformers (LVDTs), and linear potentiometers – were calibrated prior to testing through an in-house calibration procedure, which involved comparison against a reference sensor previously calibrated at an officially accredited metrology institution to ensure measurement accuracy. Before the commencement of the experimental campaign, a comprehensive visual and mechanical inspection of the shaking table infrastructure was carried out to verify its operational integrity. This verification was further reinforced by comparing the commanded input excitations with the actual recorded motions of the bare shaking table (i.e., without any structural load), which demonstrated a correlation exceeding 99%. This high level of agreement confirms the precision and reliability of the actuation and control systems.

During the course of testing, the severity of seismic inputs and high-amplitude excitations caused some transducers to operate beyond their measurement range, resulting in signal saturation. To ensure data reliability, cross-validation of all sensor outputs was conducted independently by multiple authors. This process identified a limited number of erroneous signals, primarily originating from strain gauges embedded in reinforcement bars. Some of these gauges were damaged during the concreting process, while others were affected by water

Fig. 21 Model 2. Instrumentation setup – Phase 1.

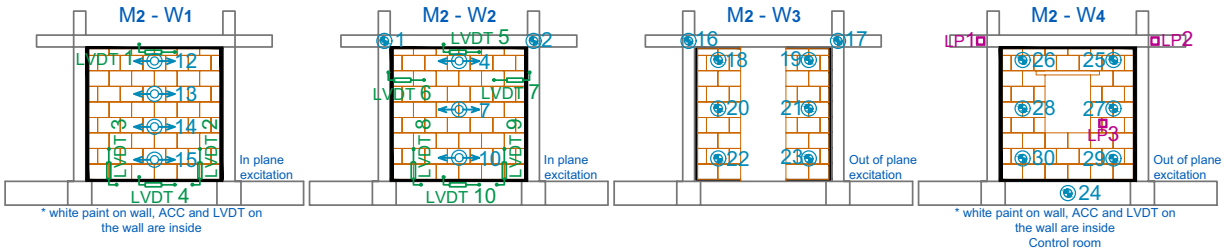

Fig. 22 Model 2. Instrumentation setup – Phase 1. Positions of accelerometers (ACC), linear potentiometers (LP), and linear variable differential transformers (LVDT).

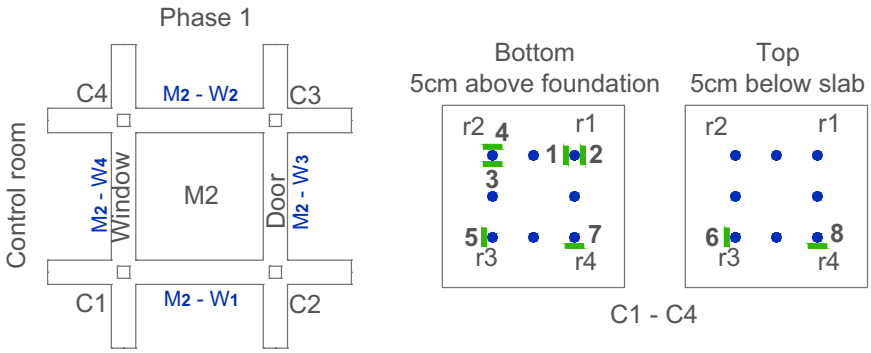

Fig. 23 Model 2. Instrumentation setup, Strain Gauges – Phase 1. *Model 2 – Shaking table tests (rotated model 90 degrees) – Phase 2.*

infiltration at the gauge surface, which compromised signal stability. To compensate for such anticipated failures, a higher-than-necessary number of strain gauges was installed during model preparation.

Additional measurement inconsistencies were attributed to noise contamination from high-frequency components and direct current (DC) offsets present in certain channels. These issues were addressed using standard

Fig. 24 Model 2. Instrumentation setup – Phase 2.

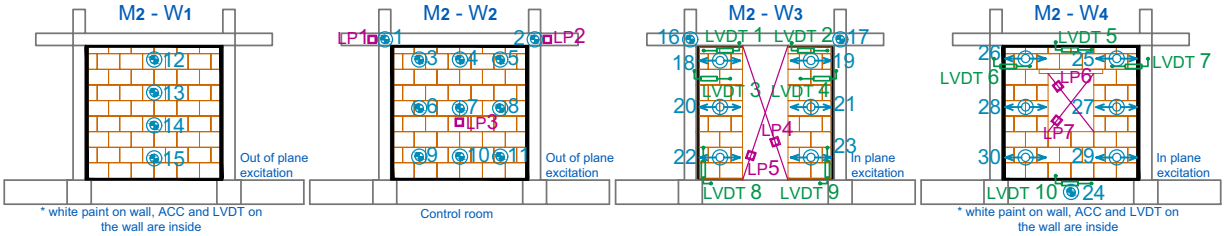

Fig. 25 Model 2. Instrumentation setup – Phase 2. Positions of accelerometers (ACC), linear potentiometers (LP), and linear variable differential transformers (LVDT).

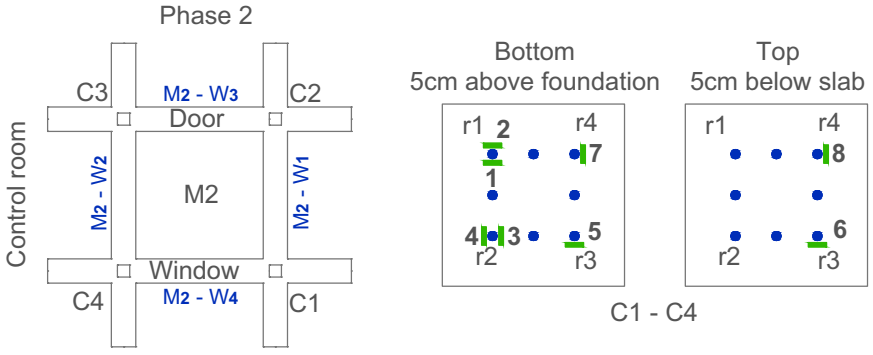

Fig. 26 Model 2. Instrumentation setup, Strain Gauges – Phase 2.

signal processing techniques, including filtering and frequency domain analysis, which were applied during post-processing to improve data quality and eliminate non-physical artifacts.

Prior to testing, the DIC system was calibrated using a 2500 × 2500 mm² calibration grid, enabling high-accuracy measurement of large surfaces. Calibration precision was within 0.017 pixels, with a spatial measurement accuracy of 0.019 mm.

Code availability

The scripts developed for opening and visualizing the dataset are publicly available in the GitHub repository ERIES-FLEJOI-TestData (https://github.com/alessandrolotti/ERIES-FLEJOI-TestData). The repository also includes detailed instructions for executing the scripts and replicating the visualizations.

Received: 30 December 2024; Accepted: 2 July 2025;
Published online: 19 July 2025

References

1. Del Vecchio, C. *et al*. Repair costs of existing RC buildings damaged by L'Aquila earthquake and comparison with FEMA P-58 predictions. *Earthquake Spectra* **34**(1), 237–63 (2018).
2. Elgawady M, Lestuzzi P, Badoux M. A review of conventional seismic retrofitting techniques for URM. In: *13th international brick and block masonry conference*; 1–10 (2004).
3. Koutas, L., Bousias, S. N. & Triantafillou, T. C. Seismic strengthening of masonry-infilled RC frames with TRM: experimental study. *Journal of Composites for Construction* **19**(2), 04014048 (2015).
4. De Santis, S., De Canio, G., de Felice, G., Meriggi, P. & Roselli, I. Out-of-plane seismic retrofitting of masonry walls with Textile Reinforced Mortar composites. *Bulletin of Earthquake Engineering*, **17**(11), 6265–6300 (2019a).
5. Kallioras, S. *et al*. Cross-laminated timber for seismic retrofitting of RC buildings: Substructured pseudodynamic tests on a full-scale prototype. *Earthquake Engineering & Structural Dynamics*, **53**(14), 4354–4378 (2024a).
6. Furtado, A., Rodrigues, H., Arêde, A. & Varum, H. Experimental tests on strengthening strategies for masonry infill walls: A literature review. *Construction and Building Materials* **263**, 120520 (2020).
7. De Santis, S. *et al*. Out-of-plane seismic retrofitting of masonry walls with Textile Reinforced Mortar composites. *Bulletin of Earthquake Engineering* **17**, 6265–6300, https://doi.org/10.1007/s10518-019-00701-5 (2019b).
8. Kallioras, S. *et al*. (2024b). Cross-laminated timber for seismic retrofitting of RC buildings: Substructured pseudodynamic tests on a full-scale prototype. *Earthquake Engineering and Structural Dynnamics*. **53**, 4354–4378, https://doi.org/10.1002/eqe.4222 (2024).
9. Andre Furtado, H, R. & Antonio Arede, H. V. Experimental tests on strengthening strategies for masonry infill walls: A literature review. *Construction and Building Materials*, **263**, 120520, ISSN 0950-0618, https://doi.org/10.1016/j.conbuildmat.2020.120520 (2020).
10. Da Porto, F., Verlato, N., Guidi, G. & Modena, C. The INSYSME project: Innovative construction systems for earthquake resistant masonry infill walls. In *Brick and block masonry: Proceedings of the 16th International Brick and Block Masonry Conference, Padova, Italy*, 26–30 June 2016 (pp. 6). CRC Press. https://doi.org/10.1201/b21889 (2016).
11. Ahmadi, H., Dusi, A. & Gough, J. A rubber-based system for damage reduction in infill masonry walls. In: *16th World conference on earthquake engineering*, 16WCEE, Santiago, Chile (01. 09-13. 2017) (2017).
12. Verlato, N. Development of a clay masonry enclosure system with deformable joints: experimental analysis and numerical. Università Degli Studi Di Brescia. *Doctoral dissertation* (2017).
13. Dhir, P. K., Tubaldi, E., Orfeo, A. & Ahmadi, H. Cyclic shear behaviour of masonry triplets with rubber joints. *Construction and Building Materials*. **351**, 128356 (2022a).
14. Dhir, P. K., Tubaldi, E., Ahmadi, H. & Gough, J. Numerical modelling of reinforced concrete frames with masonry infills and rubber joints. *Engineering Structures* **246**, 112833 (2021).
15. Dhir, P. K., Tubaldi, E., Pantò, B. & Caliò, I. A macro-model for describing the in-plane seismic response of masonry-infilled frames with sliding/flexible joints. *Earthquake Engineering and Structural Dynamics*. **51**(12), 3022–3044, https://doi.org/10.1002/eqe.3714 (2022b).
16. Marinković, M. & Butenweg, C. Innovative decoupling system for the seismic protection of masonry infill walls in reinforced concrete frames. *Engineering Structures* **197**, 109435 (2019).
17. Marinković, M. & Butenweg, C. Experimental testing of decoupled masonry infills with steel anchors for out-of-plane support under combined in-plane and out-of-plane seismic loading. *Construction and Building Materials* **318**, 126041, https://doi.org/10.1016/j.conbuildmat.2021.126041 (2022a).
18. Preti, M., Bettini, N. & Plizzari, G. Infill walls with sliding joints to limit infill-frame seismic interaction: large-scale experimental test. *Journal of Earthquake Engineering* **16**(1), 125–141 (2012).
19. Morandi, P., Milanesi, R. R. & Magenes, G. Innovative solution for seismic-resistant masonry infills with sliding joints: in-plane experimental performance. *Engineering Structures* **176**, 719–733, https://doi.org/10.1016/j.engstruct.2018.09.018 (2018).
20. Tsantilis, A. V. & Triantafillou, T. C. Innovative seismic isolation of masonry infills using cellular materials at the interface with the surrounding RC frames. *Engineering Structures* **155**, 279–297, https://doi.org/10.1016/j.engstruct.2017.11.025 (2018).
21. Peng, Q., Zhou, X. & Yang, C. Influence of connection and constructional details on masonry-infilled RC frames under cyclic loading. *Soil Dynamics and Earthquake Engineering* **108**, 96–110 (2018).
22. European Union's Horizon Europe Framework programme under grant agreement No [101058684] (Engineering Research Infrastructures for European Synergies-ERIES.
23. Marinković, M. & Butenweg, C. Numerical analysis of the in-plane behaviour of decoupled masonry infilled RC frames. *Engineering Structures* **272**, 114959, https://doi.org/10.1016/j.engstruct.2022.114959 (2022b).
24. Milijaš, A., Marinković, M., Butenweg, C. & Klinkel, S. Experimental results of reinforced concrete frames with masonry infills with and without openings under combined quasi-static in-plane and out-of-plane seismic loading. *Bulleting of Earthquake Engineering* **21**, 3537–3579, https://doi.org/10.1007/s10518-023-01664-4 (2023).
25. Milijaš, A., Marinković, M., Butenweg, C. & Klinkel, S. Experimental investigation on the seismic performance of reinforced concrete frames with decoupled masonry infills: considering in-plane and out-of-plane load interaction. *Bulleting of Earthquake Engineering* **22**, 7489–7546, https://doi.org/10.1007/s10518-024-02012-w (2024).
26. Morandi, P. *et al*. Dynamic shaking table out-of-plane tests on weak masonry infills with and without previous in-plane loading. *Journal of Building Engineering* **100**, 111670 (2025).
27. Milanesi, R. R., Morandi, P., Manzini, C. F., Albanesi, L. & Magenes, G. Out-of-plane response of an innovative masonry infill with sliding joints from shaking table tests. *Journal of Earthquake Engineering* **26**(4), 1789–1823 (2022).
28. Rousakis, T. *et al*. Deformable Polyurethane Joints and Fibre Grids for Resilient Seismic Performance of Reinforced Concrete Frames with Orthoblock Brick Infills. *Polymers*. **12**(12), 2869, https://doi.org/10.3390/polym12122869 (2020).
29. European Committee for Standardization. EN 12390-3: Testing hardened concrete – Part 3: Compressive strength of test specimens. CEN (2009).
30. International Organization for Standardization. EN ISO 15630-1: Steel for the reinforcement and prestressing of concrete – Test methods – Part 1: Reinforcing bars, wire rod and wire. ISO (2010).
31. Tubaldi, E. *et al*. FLExible JOInts for seismic-resilient design of masonry-infilled RC frames [Data set]. *Zenodo*. https://doi.org/10.5281/zenodo.13838081 (2024).
32. Carl Zeiss, A. G. (n.d.). *ARAMIS Adjustable 24 M*. ZEISS Industrial Quality Solutions. https://www.zeiss.com/metrology/en/systems/optical-3d/3d-testing/aramis-adjustable-24m.html Retrieved May 8, 2025.

33. Carl Zeiss, A. G. (n.d.). *ZEISS Correlate*. ZEISS Industrial Quality Solutions. https://www.zeiss.com/metrology/en/software/zeiss-correlate.html Retrieved May 8, 2025.
34. National Instruments. (n.d.). The NI TDMS file format. NI. https://www.ni.com/en/support/documentation/supplemental/06/the-ni-tdms-file-format.html Retrieved April 30, 2025.
35. National Instruments. (n.d.). TDMS file format internal structure. NI. https://www.ni.com/en/support/documentation/supplemental/07/tdms-file-format-internal-structure.html Retrieved April 30, 2025.
36. Shafranovich, Y. Common format and MIME type for comma-separated values (CSV) files (RFC 4180). *Internet Engineering Task Force*. https://www.rfc-editor.org/rfc/rfc4180 (2005).

Acknowledgements

This work is part of the transnational access project "ERIES-FLEJOI", supported by the Engineering Research Infrastructures for European Synergies (ERIES) project (www.eries.eu), which has received funding from the European Union's Horizon Europe Framework Programme under Grant Agreement No. 101058684. This is ERIES publication number D5. We also wish to acknowledge the valuable contributions of the experts and professionals who generously shared their knowledge and expertise, playing a crucial role in the project's success.

Author contributions

Enrico Tubaldi served as the Principal Investigator of the project, developing the overarching research agenda, securing the funding, and supervising the team throughout the entire duration of the project, with support from the co-authors. Filip Manojlovski prepared the initial draft of the manuscript, which underwent a first round of review by Aleksandra Bogdanovic and Fabio Freddi, followed by a final review and editorial input from Enrico Tubaldi. Enrico Tubaldi also coordinated the iterative revision process in collaboration with all co-authors. Igor Markovski and Nikola Naumovski were responsible for conducting the experimental tests, while Dejan Filipovski oversaw data acquisition. Data processing and cleaning were carried out by Alessandro Lotti and Dejan Filipovski. All authors contributed to the writing, critical revision, and final proofreading of the manuscript.

Competing interests

The authors declare no competing interests.

Additional information

Correspondence and requests for materials should be addressed to F.M. or E.T.